between a slope and a flat terrain showing a regular topography in OSIRIS images (*31*). The morphology and illumination conditions at this place are similar to those of many nearby areas observed by VIRTIS-M.

The presence of CO_2 ice at the surface of the nucleus thus appears to be an ephemeral occurrence, which provides clues to the emplacement mechanism. After perihelion passage, the activity of a cometary nucleus starts to decrease, with water sublimation decreasing first. Nucleus thermodynamical modeling (*1*) shows that a stratigraphy associated to the volatility of the major gaseous species is produced in the outer layers of 67P/CG. However, the combination of spin axis inclination and nucleus shape means that the Anhur CO_2 ice–rich area experiences a fast drop in illumination, going into permanent shadow quickly after equinox and, consequently, undergoing a rapid reduction in surface temperatures in winter to less than 80 K, whereas the interior remains warmer for a longer time because of the low thermal inertia (*8*, *29*). Sublimation of water ice at depth is prevented, but sublimation of CO_2 ice is not; CO_2 can continue to flow from the interior to the surface, where it begins to freeze as a result of the low surface temperatures. Moving further toward the aphelion, the low surface temperatures preserve the CO_2 ice on the surface, which grows in >100-μm grains until, on the next orbit, it is exposed again to sunlight and sublimates away. This inverse temperature profile of cometary surfaces (warmer inside and cooler on the surface) going into winter after perihelion (in permanently shadowed regions) could potentially freeze other volatiles that are sublimed from the warmer interior as well. Based on the temperature of these surface areas, more volatiles species such as CO and CH_4 could also be frozen until the next exposure to solar photons occurs. The same phenomenon could also explain why no water ice was seen at this site during the initial exposure to the Sun, because the water ice would have been frozen at lower depths than the CO_2 ice.

The 67P/CG nucleus shows two different temporal activity cycles respectively caused by H_2O and CO_2 ices in different regions: Whereas water ice has diurnal variability, with a surface sublimation and condensation cycle occurring in the most active areas (*7*), the surface condensation of CO_2 ice has a seasonal dependence. Similar processes are probably common among many Jupiter-family comets, which share with 67P/CG short revolution periods and eccentric orbits (*32*).

REFERENCES AND NOTES

1. M. C. De Sanctis, M. T. Capria, A. Coradini, *Adv. Space Res.* **38**, 1906–1910 (2006).
2. M. Hässig *et al.*, *Science* **347**, aaa0276 (2015).
3. D. Bockelée-Morvan *et al.*, *Astron. Astrophys.* **583**, A6 (2015).
4. A. Migliorini *et al.*, *Astron. Astrophys.* **589**, A45 (2016).
5. N. Fougere *et al.*, *Astron. Astrophys.* **588**, A134 (2016).
6. U. Fink *et al.*, *Icarus* **277**, 78–97 (2016).
7. M. C. De Sanctis *et al.*, *Nature* **525**, 500–503 (2015).
8. M. Choukroun *et al.*, *Astron. Astrophys.* **583**, A28 (2015).
9. F. Preusker *et al.*, *Astron. Astrophys.* **583**, A33 (2015).
10. A. Coradini *et al.*, *Space Sci. Rev.* **128**, 529–559 (2007).
11. M. R. El-Maarry *et al.*, *Astron. Astrophys.* **593**, A110 (2016).
12. Materials and methods are available as supplementary materials on *Science* Online.
13. B. Hapke, *Theory of Reflectance and Emittance Spectroscopy* (Cambridge Univ. Press, 2012).
14. M. Ciarniello *et al.*, *Icarus* **214**, 541–555 (2011).
15. F. Capaccioni *et al.*, *Science* **347**, aaa0628 (2015).
16. M. Ciarniello *et al.*, *Astron. Astrophys.* **583**, A31 (2015).
17. E. Quirico, B. Schmitt, *Icarus* **127**, 354–378 (1997).
18. E. Quirico *et al.*, *Icarus* **139**, 159–178 (1999).
19. E. Quirico *et al.*, *Icarus* **272**, 32–47 (2016).
20. S. G. Warren, *Appl. Opt.* **23**, 1206 (1984).
21. R. M. Mastrapa, S. A. Sandford, T. L. Roush, D. P. Cruikshank, C. M. Dalle Ore, *Astrophys. J.* **701**, 1347–1356 (2009).
22. R. N. Clark *et al.*, *Icarus* **218**, 831–860 (2012).
23. G. Filacchione *et al.*, *Nature* **529**, 368–372 (2016a).
24. G. Filacchione *et al.*, *Icarus* **274**, 334–349 (2016b).
25. F. Tosi *et al.*, *Icarus* **240**, 36–57 (2014).
26. W. F. Huebner, J. Benkhoff, M-T. Capria, A. Coradini, C. De Sanctis, R. Orosei, D. Prialnik, "Heat and gas diffusion in comet nuclei" (International Space Science Institute report SR-004, ESA Publications Division, 2006).
27. L. Jorda, R. H. Gaskell, Shape models of 67P/Churyumov-Gerasimenko, RO-C-OSINAC/OSIWAC-5-67P-SHAPE-V1.0 (NASA Planetary Data System and ESA Planetary Science Archive, 2015); https://pds.nasa.gov/ds-view/pds/viewProfile.jsp?dsid=RO-C-OSINAC/OSIWAC-5-67P-SHAPE-V1.0.
28. L. Jorda *et al.*, *Icarus* **277**, 257–278 (2016).
29. F. P. Schloerb *et al.*, *Astron. Astrophys.* **583**, A29 (2015).
30. D. Bockelée-Morvan *et al.*, *Mon. Not. R. Astron. Soc.* 10.1093/mnras/stw2428 (2016).
31. S. Fornasier *et al.*, *Science* **354**, 1566–1570 (2016).
32. D. Jewitt, *Earth Moon Planets* **79**, 35–53 (1997).

ACKNOWLEDGMENTS

The authors thank the institutions and agencies that supported this work: the Italian Space Agency (ASI), Centre National d'Etudes Spatiales (CNES, France), DLR (Germany), and NASA (USA). VIRTIS was built by a consortium from Italy, France, and Germany, under the scientific responsibility of INAF-IAPS, Rome, Italy, which also led the scientific operations. The VIRTIS instrument development for ESA has been funded and managed by ASI, with contributions from Observatoire de Meudon (financed by CNES) and DLR. The VIRTIS instrument industrial prime contractor was formerly Officine Galileo and is now Leonardo SpA in Campi Bisenzio, Florence, Italy. The authors thank the Rosetta Liaison Scientists, the Rosetta Science Ground Segment, and the Rosetta Mission Operations Centre for their support in planning the VIRTIS observations. T.M. acknowledges additional funding from NASA JPL, W.-H.I. from the National Science Council of Taiwan (grant 102-2112-M-008-013-MY3) and Science and Technology Development Fund of Macao Special Administrative Region (grant 017/2014/A1), and L.M. from Deutsche Forschungsgemeinschaft (grant MO 3007/1-1). The VIRTIS calibrated data are available through ESA's Planetary Science Archive (www.cosmos.esa.int/web/psa/rosetta). This research has made use of NASA's Astrophysics Data System.

SUPPLEMENTARY MATERIALS

www.sciencemag.org/content/354/6319/1563/suppl/DC1
Materials and Methods
Figs. S1 to S8
Table S1
References (*33*–*41*)

8 June 2016; accepted 28 October 2016
Published online 17 November 2016
10.1126/science.aag3161

COMETARY SCIENCE

Rosetta's comet 67P/Churyumov-Gerasimenko sheds its dusty mantle to reveal its icy nature

S. Fornasier,[1]* S. Mottola,[2] H. U. Keller,[2,3] M. A. Barucci,[1] B. Davidsson,[4] C. Feller,[1] J. D. P. Deshapriya,[1] H. Sierks,[5] C. Barbieri,[6] P. L. Lamy,[7] R. Rodrigo,[8,9] D. Koschny,[10] H. Rickman,[11,12] M. A'Hearn,[13] J. Agarwal,[5] J.-L. Bertaux,[14] I. Bertini,[6] S. Besse,[15] G. Cremonese,[16] V. Da Deppo,[17] S. Debei,[18] M. De Cecco,[19] J. Deller,[5] M. R. El-Maarry,[20] M. Fulle,[21] O. Groussin,[22] P. J. Gutierrez,[8] C. Güttler,[5] M. Hofmann,[5] S. F. Hviid,[2] W.-H. Ip,[23,24] L. Jorda,[22] J. Knollenberg,[2] G. Kovacs,[5,25] R. Kramm,[5] E. Kührt,[2] M. Küppers,[15] M. L. Lara,[8] M. Lazzarin,[6] J. J. Lopez Moreno,[8] F. Marzari,[6] M. Massironi,[26,27] G. Naletto,[28,27,17] N. Oklay,[5] M. Pajola,[29,27] A. Pommerol,[20] F. Preusker,[2] F. Scholten,[2] X. Shi,[5] N. Thomas,[20] I. Toth,[30] C. Tubiana,[5] J.-B. Vincent[5]

The Rosetta spacecraft has investigated comet 67P/Churyumov-Gerasimenko from large heliocentric distances to its perihelion passage and beyond. We trace the seasonal and diurnal evolution of the colors of the 67P nucleus, finding changes driven by sublimation and recondensation of water ice. The whole nucleus became relatively bluer near perihelion, as increasing activity removed the surface dust, implying that water ice is widespread underneath the surface. We identified large (1500 square meters) ice-rich patches appearing and then vanishing in about 10 days, indicating small-scale heterogeneities on the nucleus. Thin frosts sublimating in a few minutes are observed close to receding shadows, and rapid variations in color are seen on extended areas close to the terminator. These cyclic processes are widespread and lead to continuously, slightly varying surface properties.

All cometary nuclei observed to date have appeared to be dark, with only a limited amount of water ice detected in small patches (*1*, *2*), although water is the dominant volatile observed in their coma.

The Rosetta spacecraft has been orbiting comet 67P/Churyumov-Gerasimenko since August 2014, providing the opportunity to continuously investigate its nucleus. The comet has a distinct bilobate shape and a complex morphology (*3*–*5*), with a

surface dominated by anhydrous and organic-rich refractory materials (*6*). Small amounts of water ice have been identified by the Visible, Infrared, and Thermal Imaging Spectrometer (VIRTIS) spectrometer in different regions (*7*–*9*), and several isolated or clustered bright spots were observed in Optical, Spectroscopic, and Infrared Remote Imaging System (OSIRIS) images and interpreted as exposures of dirty water ice (*9*, *10*).

Here, we report on seasonal and diurnal color variations of the surface of 67P's nucleus from observations with the narrow-angle-camera (NAC) of the OSIRIS imaging system (*11*) onboard Rosetta, as caused by the evolution of the dust mantle and exposures of water ice.

We monitored the color evolution of the nucleus from 3.6 astronomical units (AU) to perihelion (1.24 AU) and beyond by measuring changes in the spectral slope in the 535- to 882-nm range. Comparing the spectral slopes obtained in late August 2015, shortly after perihelion passage, with those obtained in early August 2014 after phase reddening correction (*12*) (Fig. 1, figs. S1 to S3, and table S1) clearly indicates that the nucleus has become relatively bluer—i.e., the spectral slope has decreased as the comet approached perihelion.

Even though only the equatorial regions such as Imhotep (*13*) are common for both data sets (Figs. 1 and fig. S4), due to different seasonal insolation conditions, a decrease of about 30% in the mean spectral slope (*12*) from 3.6 AU to the perihelion passage is measured in the common areas. A decrease of the visible spectral slope was also reported from VIRTIS observations in the August to November 2014 time frame (*14*). In a water-ice/refractory-material mixture, regions with bluer colors indicate a higher abundance of water ice (*15*, *16*), as demonstrated by VIRTIS observations (*8*, *9*) and as previously observed for the 9P/Tempel 1 and 103P/Hartley 2 comets (*1*, *2*).

In addition to the change of color, the amount of phase reddening (the increase of spectral slope with phase angle) decreased by a factor of two when the comet approached perihelion in the 2015 observations compared with those from August 2014 (*12*, *15*), indicating a change in the physical properties of the outermost layer of the nucleus. The relatively blue color of the surface and the decreased phase reddening effect observed at small heliocentric distances suggest that the increasing level of activity has thinned the surface dust coating, partially exposing the underlying ice-rich layer. This result is in agreement with the variation of the sublimation rate with heliocentric distance r reported by (*17*), considerably steeper ($\propto r^{-4.2}$) than the one obtained from modeling considering the shape of the nucleus and seasonal effects (*18*). This steepness can be explained by the observed thinning of the surface dust layer that facilitates the sublimation during the approach to perihelion. Observations at 2.2 AU outbound (fig. S3) show that the comet's colors redden again as the activity decreases and is no longer capable of sustained removal of dust.

The increase in water-ice visibility is observed on the whole surface, indicating that the composition in terms of dust-to-ice ratio must be similar at large scales all over the nucleus. This means that even the smooth areas commonly thought to be covered with material that fell back on the surface (*18*) must be water-ice rich.

We observed and monitored two bright patches, of about 1500 m^2 each (table S2), located in a smooth area of the Anhur/Bes (*13*) regions (Fig. 2 and fig. S4), on images acquired on 27 April to 2 May 2015. One of the two patches, patch B in Fig. 2, was still present in an image acquired on 7 May, yielding a survival time of at least 5 to 10 days. These features are considerably larger than the meter-scale bright spots previously detected on the 67P comet (*10*). The VIRTIS spectrometer detected the presence of CO_2 ice in region A on 21 to 23 March 2015 that had sublimated in less than 3 weeks (*19*). On 12 April, the bright patches were not present yet, but these regions were spectrally bluer than the surrounding ones, indicating a higher water-ice abundance (Fig. 2). On 27 April and 2 May, the bright patches were clearly visible and showed a relatively flat spectrum, with a maximum reflectance four to six times as bright as the surrounding regions. A water-ice surface abundance of ~25% linearly mixed with the comet

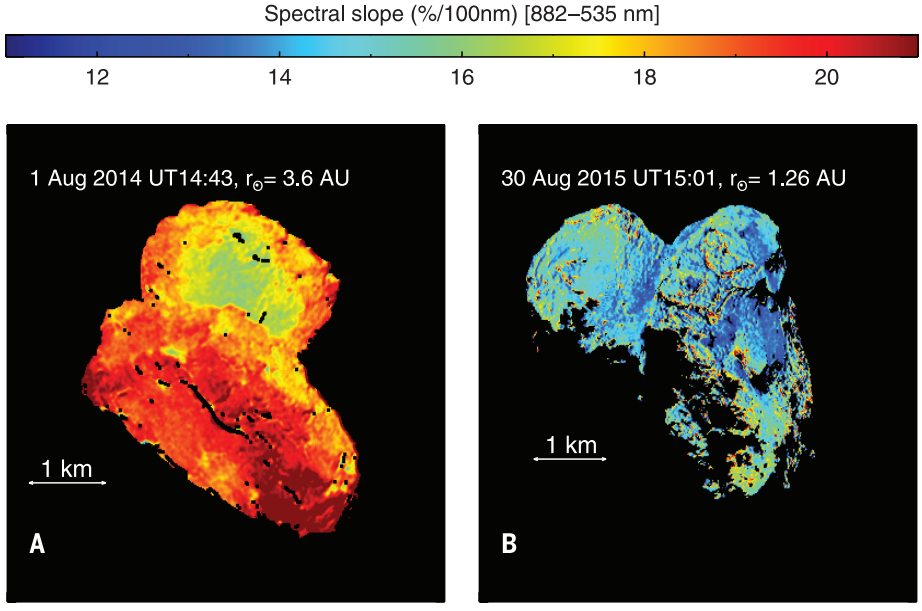

Fig. 1. Spectral slope evolution with heliocentric distance. The August 2014 image was corrected for the phase reddening from 10° to 70° using the coefficients published in (*15*) to match the viewing geometry on the right. See fig. S4 for the morphological regions context.

[1]Laboratoire d'Etudes Spatiales et d'Instrumentation en Astrophysique (LESIA), Observatoire de Paris, PSL Research University, CNRS, Université Paris Diderot, Sorbonne Paris Cité, UPMC Université Paris 06, Sorbonne Universités, 5 Place J. Janssen, Meudon Principal Cedex 92195, France. [2]Deutsches Zentrum für Luft- und Raumfahrt (DLR), Institut für Planetenforschung, Asteroiden und Kometen, Rutherfordstrafle 2, 12489 Berlin, Germany. [3]Institut für Geophysik und Extraterrestrische Physik (IGEP), Technische Universität Braunschweig, Mendelssohnstrasse 3, 38106 Braunschweig, Germany. [4]Jet Propulsion Laboratory, M/S 183-301, 4800 Oak Grove Drive, Pasadena, CA 91109, USA. [5]Max-Planck-Institut für Sonnensystemforschung, Justus-von-Liebig-Weg, 3, 37077, Göttingen, Germany. [6]Department of Physics and Astronomy, University of Padova, Vicolo dell'Osservatorio 3, 35122 Padova, Italy. [7]Laboratoire d'Astrophysique de Marseille, UMR 7326 CNRS and Université Aix-Marseille, 38 Rue Frédéric Joliot-Curie, 13388 Marseille Cedex 13, France. [8]Instituto de Astrofisica de Andalucia (CSIC), c/ Glorieta de la Astronomia s/n, 18008 Granada, Spain. [9]International Space Science Institute, Hallerstrasse 6, 3012 Bern, Switzerland. [10]Scientific Support Office, European Space Research and Technology Centre/ESA, Keplerlaan 1, Postbus 299, 2201 AZ Noordwijk ZH, Netherlands. [11]Department of Physics and Astronomy, Uppsala University, Box 516, 75120 Uppsala, Sweden. [12]Polish Academy of Sciences, Space Research Center, Bartycka 18A, 00716 Warszawa, Poland. [13]Department of Astronomy, University of Maryland, College Park, MD 20742-2421, USA. [14]Laboratoire Atmosphères, Milieux, Observations Spatiales (LATMOS) CNRS/UVSQ/IPSL, 11 Boulevard d'Alembert, 78280, Guyancourt, France. [15]Operations Department, European Space Astronomy Centre/ESA, P.O. Box 78, 28691 Villanueva de la Canada, Madrid, Spain. [16]Istituto Nazionale di Astrofisica (INAF), Osservatorio Astronomico di Padova, Vicolo dell'Osservatorio 5, 35122 Padova, Italy. [17]CNR-IFN UOS Padova LUXOR, Via Trasea, 7, 35131 Padova, Italy. [18]Department of Mechanical Engineering – University of Padova, via Venezia 1, 35131 Padova, Italy. [19]University of Trento, Via Mesiano 77, 38100 Trento, Italy. [20]Physikalisches Institut der Universität Bern, Sidlerstrasse 5, 3012 Bern, Switzerland. [21]INAF, Osservatorio Astronomico, Via Tiepolo 11, 34014 Trieste, Italy. [22]Aix Marseille Université, CNRS, LAM (Laboratoire d'Astrophysique de Marseille), UMR 7326, 38 Rue Frédéric Joliot-Curie, 13388 Marseille Cedex 13, France. [23]Graduate Institute of Astronomy, National Central University, 300 Chung-Da Rd, Chung-Li 32054 Taiwan. [24]Space Science Institute, Macau University of Science and Technology, Macau, China. [25]Budapest University of Technology and Economics, Budapest, Hungary. [26]Dipartimento di Geoscienze, University of Padova, Via G. Gradenigo 6, 35131 Padova, Italy. [27]Center of Studies and Activities for Space (CISAS), G. Colombo, University of Padova, Via Venezia 15, 35131 Padova, Italy. [28]University of Padova, Department of Information Engineering, Via Gradenigo 6/B, 35131 Padova, Italy. [29]NASA Ames Research Center, Moffett Field, CA 94035, USA. [30]MTA CSFK Konkoly Observatory, Konkoly Thege M. ut 15-17, H1121 Budapest, Hungary.
***Corresponding author. Email: sonia.fornasier@obspm.fr**

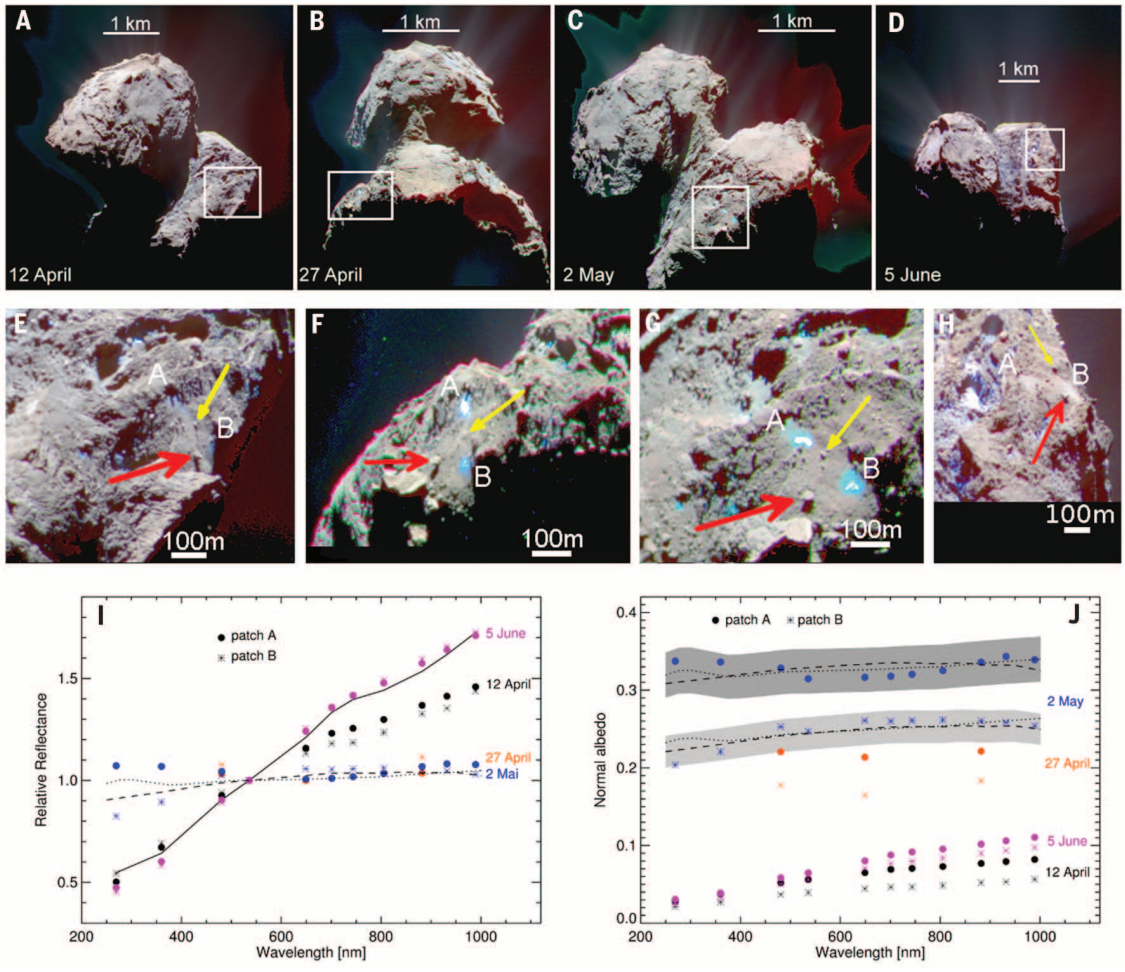

Fig. 2. Anhur/Bes ice-rich patches. Composite images (882, 649, and 480 nm filters) showing the appearance of the bright patches in the Anhur/Bes regions (**A** to **D**), and associated zooms (**E** to **H**); the arrows indicate two common boulders. The reflectance relative to 535 nm and the normal albedo are represented in (**I**) and (**J**). The black line represents the mean spectrum of the comet from a region close to the patches. Dashed and dotted lines (J) show the best-fit spectral models to the patches (associated uncertainty shown in gray) produced by the linear mixture of the comet dark terrain (*12*) enriched with 21 ± 3% of water ice (dashed line) or 23 ± 3% of water frost (dotted line) for patch B, and with 29 ± 3% of water ice (dashed line) or 32 ± 3% of water frost (dotted line) for patch A.

dark terrain is needed to match the patches' reflectance (*12*). Subsequent images covering the Anhur region were acquired on 4 to 5 June, revealing that the water ice had fully sublimated from the surface, leaving a layer spectrally indistinguishable from the average nucleus (Fig. 2).

We compute the sublimation rate for this period by applying the thermal model described in (*18*) for both intimate and areal mixtures of refractory material and ice (*12*). The estimated ice loss rate ranged from 1.4 to 2.5 kg day^{-1} m^{-2} for the intimate mixture and from 0.14 to 0.38 kg day^{-1} m^{-2} for the areal mixture cases. By noting that the permanence of the ice patches was about 10 days, we estimate a solid-ice equivalent thickness between 1.5 and 27 mm for the ice patches. The actual thickness of this layer will be up to a factor of 10 higher due to porosity of the dust/ice mixture.

The appearance and disappearance of water-ice patches shows that the level of activity is varying on time scales that are short compared with seasonal changes of the illumination. These ice-rich patches indicate a variation of the water-ice content in the uppermost layers, pointing to local compositional heterogeneities with scales of 10s of meters on 67P's nucleus. The huge width-to-depth ratio observed in the ice patches would suggest a near-surface solar-driven process being responsible for enhancement of local ice abundance, resulting from the recondensation of volatiles and sintering of the subsurface material during previous perihelion passages. Laboratory results from Kometen Simulation (KOSI) experiments had shown that a considerable fraction of sublimating ice can be redeposited instead of being released through the dust mantle (*20*). Numerical simulations show that a hardened layer may form beneath a fine dust mantle (*21*), a hard layer that was detected by the Philae lander in the Abydos site (*22*). The composition of the icy patches may be representative of the comet's near surface. Occasional local removal of the overlying mantling material could expose the underlying layer, leading to an icy surface for limited periods of time.

Approaching perihelion, the nucleus has shown considerable diurnal color variations on extended areas and the occurrence of water frost close to morning shadows. This is evident on the Imhotep region, where morphological changes were observed (*23*). Areas just emerging from the shadows are spectrally bluer than their surroundings (Fig. 3A), while 40 min later, once fully illuminated, their spectral slope has increased (Fig. 3B). This phenomenon, observed during other color sequences acquired in June and July 2015, and seen at dawn on different areas on both lobes of the comet (*12*) (fig. S5 and movie S1), is periodic. We interpret the relatively blue surface at dawn as the presence of additional water frost that condensed during the previous night.

We also observe the presence of fronts of bright material in the illuminated regions close to rapidly traveling shadows cast by local topography (Fig. 3). A water-rich fringe near shadows at the Hapi/Hathor transition was also observed by VIRTIS (*7*). The bright fronts move with the shadows. Modeling of the illumination (fig. S6 and movie S2) shows that the extent of these bright features directly correlates with the shadow travel speed, being wider where the shadow speed is faster and narrower where the shadow speed is slower.

These fronts are about six times as bright as the mean comet reflectance. Their spectrum is globally flat with a flux enhancement in the ultraviolet (Fig. 4 and fig. S7), similar to that observed on blue regions of comet Tempel 1 (*1*). An abundance of about 17% water frost linearly mixed with the comet dark terrain is needed to match the reflectance of the bright fronts (*12*). We interpret these bright features as surface frost, formed when water vapor released from the subsurface recondenses after sunset, that rapidly sublimates when exposed to the Sun. Molecules in the inner

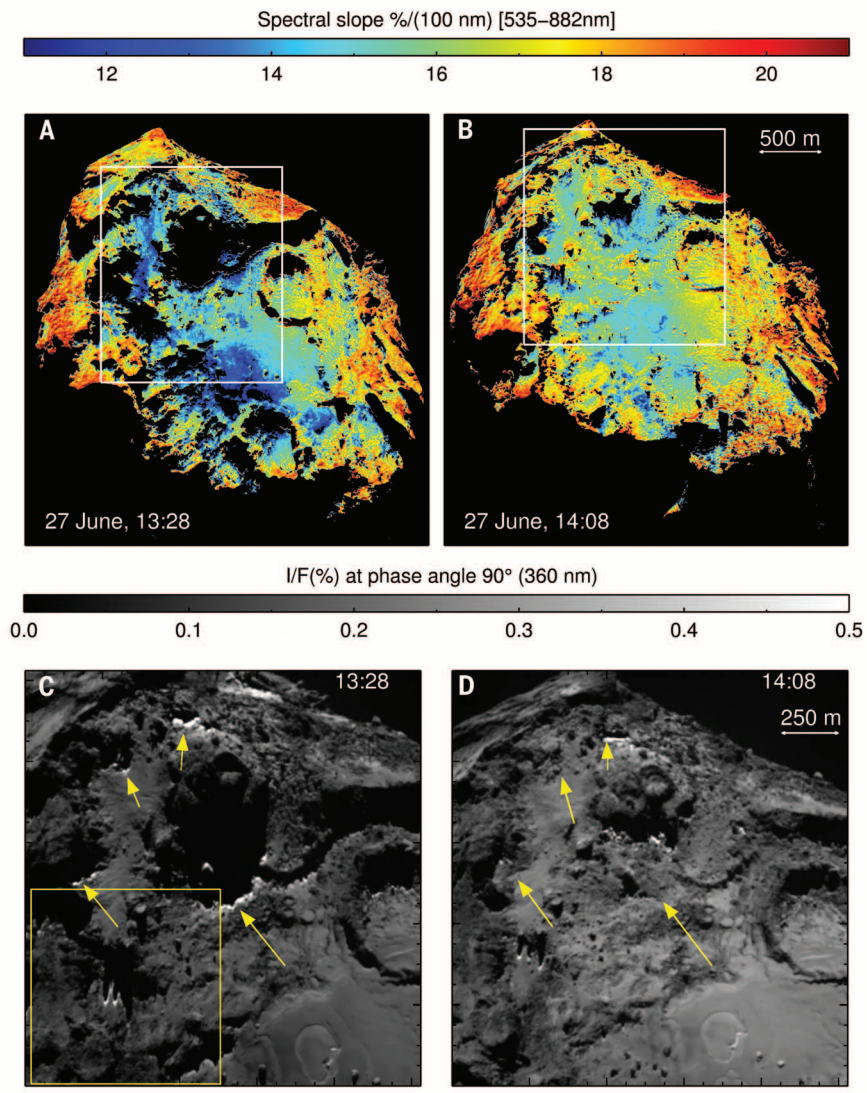

Fig. 3. Spectral slope changes and frost sublimation. (**A** and **B**) Spectral slope maps of Imhotep region taken 40 min apart. The Sun is toward the top. (**C** and **D**) Zoom in radiance factor (I/F) of the regions indicated by the white rectangle on (A) and (B) showing morning frosts (evidenced by the yellow arrows), disappearing and moving with shadows. The yellow rectangular region in (C) indicates the area where the same frost structures are seen 2 weeks later and analyzed in Fig. 4.

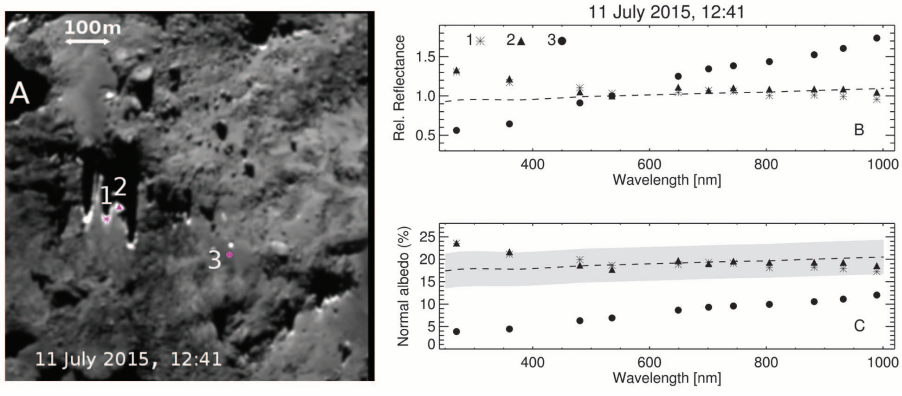

Fig. 4. Reflectance of frost fronts. (**A**) Bright fronts seen close to shadows on the Imhotep region (see Fig. 3 for the context). (**B** and **C**) Reflectance normalized at 535 nm and normal albedo of three selected regions [magenta points in (A)]. The dashed line represents the best-fit model, with uncertainties in gray, including 17 ± 4% of water frost linearly mixed to the comet dark terrain.

coma may also be back-scattered to the nucleus surface and recondense, contributing to the frost formation (*24*, *25*). From the shadow travel speed and the extent of the frost fronts, we calculate an ice permanence time of about 3 min (*12*). From thermal modeling using an intimate mixture, we estimate a water-ice sublimation rate of about 4 g m^{-2} min^{-1}, from which we infer a total ice content of about 12 g m^{-2} for the frost layer, which is extremely thin (thickness ~10 to 15 μm of equivalent solid ice) (table S3). If we assume an areal mixing, the sublimation rate and total ice content are lower by a factor of 8. In the absence of direct temperature measurements of the frost, it is impossible to discriminate whether areal or intimate mixture represents the correct thermal model (*1*). In either case, the exposed ice is depleted on short time scales. In the case of geographical mixing, however, sublimation rates at the time of the observations would be so low that a frost permanence time of 3 min would imply a frost layer on the order of ~1 μm solid-ice equivalent. Because it is questionable whether such a thin layer would be optically thick, it appears more likely that the frost patches are intimately mixed with the refractory material. Similar to the observed diurnal color variations, the recondensation of frosts is also a periodic phenomenon that takes place close to topographic shadows, as indicated in Figs. 3 and 4.

The long-term observations of 67P provide information on the composition of the outermost layers of the nucleus. They reveal that ice is abundant just beneath the surface on the whole nucleus, which, most of the time, is covered by a thin layer of dust. Hence, the apparent surface composition is globally dominated by anhydrous refractory materials (*6*). The increasing cometary activity while approaching the Sun progressively thins the dust surface layer, partially exposing the ice-richer subsurface, yielding nucleus's colors that are bluer relative to those at large heliocentric distances.

OSIRIS observations show that mixtures having high abundance (up to ~30%) of water ice are occasionally locally present on the nucleus and that the lifetime of exposed ice is short, on the order of a few minutes to a few days. However, no dust-free ice patches were observed even during the peak of activity near perihelion, indicating that water ice and dust are well mixed within the resolution limit of the images (~2 m $pixel^{-1}$). Most of the bright features are observable only at high spatial resolution and under particular insolation conditions—i.e., close to the morning shadows. Similar phenomena presumably take place on other comets, explaining why cometary nuclei are so dark even if they have important water ice abundance. The extended bright patches observed in the Anhur/Bes regions indicate a local enrichment of water ice, pointing to compositional heterogeneities in the uppermost layers of comet 67P.

REFERENCES AND NOTES

1. J. M. Sunshine *et al.*, *Science* **311**, 1453–1455 (2006).
2. J. M. Sunshine *et al.*, The Distribution of Water Ice on Comet 103P/Hartley 2. Proceedings of the conference held May 16–20, 2012, in Niigata, Japan; Lunar and Planetary Institute (LPI) Contribution no. 1667, id.6438 (2012).

3. M. Massironi *et al.*, *Nature* **526**, 402–405 (2015).
4. H. Sierks *et al.*, *Science* **347**, aaa1044 (2015).
5. N. Thomas *et al.*, *Science* **347**, aaa0440 (2015).
6. F. Capaccioni *et al.*, *Science* **347**, aaa0628 (2015).
7. M. C. De Sanctis *et al.*, *Nature* **525**, 500–503 (2015).
8. G. Filacchione *et al.*, *Nature* **529**, 368–372 (2016).
9. M. A. Barucci *et al.*, *Astron. Astrophys.* **595**, A102 (2016).
10. A. Pommerol *et al.*, *Astron. Astrophys.* **583**, A25 (2015).
11. H. U. Keller *et al.*, *Space Sci. Rev.* **128**, 433–506 (2007).
12. Materials and methods are available as supplementary materials on *Science* Online.
13. M. R. El-Maarry *et al.*, *Astron. Astrophys.* **593**, A110 (2016).
14. G. Filacchione *et al.*, *Icarus* **274**, 334–349 (2016).
15. S. Fornasier *et al.*, *Astron. Astrophys.* **583**, A30 (2015).
16. N. Oklay *et al.*, *Astron. Astrophys.* **586**, A80 (2016).
17. N. Fougere *et al.*, *Astron. Astrophys.* **588**, A134 (2016).
18. H. U. Keller *et al.*, *Astron. Astrophys.* **583**, A34 (2015).
19. G. Filacchione *et al.*, *Science* **354**, 1563–1566 (2016).
20. J. Benkhoff, K. J. Seidensticker, K. Seiferlin, T. Spohn, *Planet. Space Sci.* **43**, 353–361 (1995).
21. K. J. Kossacki, T. Spohn, A. Hagermann, E. Kührt, *Icarus* **260**, 464–474 (2015).
22. T. Spohn *et al.*, *Science* **349**, aab0464 (2015).
23. O. Groussin *et al.*, *Astron. Astrophys.* **583**, A36 (2015).
24. B. R. J. Davidsson, Y. V. Skorov, *Icarus* **168**, 163–185 (2004).
25. J. F. Crifo, *Astron. Astrophys.* **187**, 438–450 (1987).

ACKNOWLEDGMENTS

OSIRIS was built by a consortium led by the Max-Planck-Institut für Sonnensystemforschung, Göttingen, Germany, in collaboration with CISAS, University of Padova, Italy; the Laboratoire d'Astrophysique de Marseille, France; the Instituto de Astrofísica de Andalucia, CSIC, Granada, Spain; the Scientific Support Office of the European Space Agency (ESA), Noordwijk, The Netherlands; the Instituto Nacional de Técnica Aeroespacial, Madrid, Spain; the Universidad Politéchnica de Madrid, Spain; the Department of Physics and Astronomy of Uppsala University, Sweden; and the Institut für Datentechnik und Kommunikationsnetze der Technischen Universität Braunschweig, Germany. The support of the contributing research institutes of the OSIRIS consortium and of the national funding agencies of Germany (DLR), France (CNES), Italy (ASI), Spain (MEC), Sweden (SNSB), and the ESA Technical Directorate is gratefully acknowledged. M.A. acknowledges NASA funding through Jet Propulsion Laboratory contract no. 1267923 and from the Akademie der Wissenschaften zu Göttingen. W.-H.I. acknowledges the Ministry of Science and Technology, Taiwan (grant no. NSC 102-2112-M-008), and Macau University of Science and Technology (grant no. FDCT 017/2014/A1). We thank the ESA teams at European Space Astronomy Centre, European Space Operations Centre, and European Space Research and Technology Centre for their work in support of the Rosetta mission. P. H. Hasselmann and D. Perna are acknowledged for helpful discussion. Rosetta/OSIRIS data are available through the ESA's Planetary Science Archive (PSA) at www.cosmos.esa.int/web/psa/rosetta. Some images used in this paper that are not yet available at PSA can be downloaded from the MPS OSIRIS website at https://planetgate.mps.mpg.de/WebFileShare/Released_Images/Fornasier+Science.

SUPPLEMENTARY MATERIALS

www.sciencemag.org/content/354/6319/1566/suppl/DC1
Materials and Methods
Figs. S1 to S7
Tables S1 to S3
Movies S1 and S2
References (*26*–*31*)

1 June 2016; accepted 27 October 2016
Published online 17 November 2016
10.1126/science.aag2671

CATALYSIS

Selective oxidative dehydrogenation of propane to propene using boron nitride catalysts

J. T. Grant,[1] C. A. Carrero,[1] F. Goeltl,[1] J. Venegas,[2] P. Mueller,[1] S. P. Burt,[2] S. E. Specht,[1] W. P. McDermott,[1] A. Chieregato,[1] I. Hermans[1,2]*

The exothermic oxidative dehydrogenation of propane reaction to generate propene has the potential to be a game-changing technology in the chemical industry. However, even after decades of research, selectivity to propene remains too low to be commercially attractive because of overoxidation of propene to thermodynamically favored CO_2. Here, we report that hexagonal boron nitride and boron nitride nanotubes exhibit unique and hitherto unanticipated catalytic properties, resulting in great selectivity to olefins. As an example, at 14% propane conversion, we obtain selectivity of 79% propene and 12% ethene, another desired alkene. Based on catalytic experiments, spectroscopic insights, and ab initio modeling, we put forward a mechanistic hypothesis in which oxygen-terminated armchair boron nitride edges are proposed to be the catalytic active sites.

Selective oxidation technology plays a pivotal role in the modern chemical industry (*1*). The scientific challenge for partial oxidations is the prevention of consecutive overoxidation of the desired product, which is often more reactive than the parent substrate. The oxidative dehydrogenation of propane (ODHP) is a contemporary example of such a challenging reaction. Although propene is conventionally produced via steam cracking of large hydrocarbons in naphtha, the more recent trend to use shale gas as feeds to steam cracker units greatly increases the availability of low-cost ethene but also results in a gap between demand and supply of propene, as well as other higher olefins (*2*, *3*). This disparity motivates the exploration of "on-purpose" propene technologies. Even though nonoxidative propane dehydrogenation is the emerging technology used today, ODHP has the potential to improve reaction efficiency over its nonoxidative counterpart because of favorable thermodynamics (exothermic and lower reaction temperatures) and enhanced catalyst stability (prevention of coke deposition on the catalyst surface). It is estimated that the potential energy savings for moving to ODHP would be ~45% of the energy consumption (*4*, *5*). This gain in reaction efficiency, coupled with the facts that demand for propene is around 100,000 kt and its production consumes around 1 quad of energy, illustrates the potential impact of ODHP if it could be implemented on a large scale. The key scientific challenge that must be overcome remains, however, the prevention of the facile overoxidation of propene product into more thermodynamically stable CO and CO_2 (CO_x).

To date, supported vanadium oxide catalysts show the most promising activity for ODHP, owing to the favorable redox properties of the active vanadium sites (*6*, *7*). However, even after decades of research, propene selectivity remains too low, even at moderate propane conversion. As an example, at 10% propane conversion, the propene selectivity typically drops to less than 60% for such conventional catalysts. The lack of kinetic control identifies the need for the discovery of alternative materials with the ability to better control this partial oxidation (*8*).

Here, we present both hexagonal boron nitride (h-BN) and boron nitride nanotubes (BNNTs) as metal-free materials able to catalyze the ODHP reaction. Although graphene and fullerene materials are emerging as catalysts for partial alkane oxidations (*9*–*11*), BN materials, one of the "inorganic analogs" of graphene, have yet to be explored for their own catalytic activity. A supported vanadia on silica catalyst (V/SiO_2) was used in this work to make direct comparisons with the catalytic performance of BN. These materials were loaded into a quartz tube reactor heated between 460 and 500°C under flowing propane, oxygen, and nitrogen as an inert carrier gas. Reaction parameters—such as temperature, catalyst mass, total gas flow-rate, and partial pressures of propane ($P_{C_3H_8}$) and oxygen (P_{O_2})—were varied to observe changes to product distributions by sampling the reactor exhaust stream via online gas chromatography and mass spectrometry. Gas contact time with the catalyst is represented in this work as the inverse weight-hour-space-velocity {$WHSV^{-1}$ [kg-catalyst s (mol C_3H_8)$^{-1}$]}, which was varied primarily by altering the total gas flow rate.

Use of BN materials results in extraordinary selectivity to propene, among the highest reported under ODHP conditions. For instance,

[1]Department of Chemistry, University of Wisconsin—Madison, 1101 University Avenue, Madison, WI 53706, USA.
[2]Department of Chemical and Biological Engineering, University of Wisconsin—Madison, 1415 Engineering Drive, Madison, WI 53706, USA.
***Corresponding author. Email: hermans@chem.wisc.edu**

Science

Rosetta's comet 67P/Churyumov-Gerasimenko sheds its dusty mantle to reveal its icy nature

S. Fornasier, S. Mottola, H. U. Keller, M. A. Barucci, B. Davidsson, C. Feller, J. D. P. Deshapriya, H. Sierks, C. Barbieri, P. L. Lamy, R. Rodrigo, D. Koschny, H. Rickman, M. A'Hearn, J. Agarwal, J.-L. Bertaux, I. Bertini, S. Besse, G. Cremonese, V. Da Deppo, S. Debei, M. De Cecco, J. Deller, M. R. El-Maarry, M. Fulle, O. Groussin, P. J. Gutierrez, C. Güttler, M. Hofmann, S. F. Hviid, W.-H. Ip, L. Jorda, J. Knollenberg, G. Kovacs, R. Kramm, E. Kührt, M. Küppers, M. L. Lara, M. Lazzarin, J. J. Lopez Moreno, F. Marzari, M. Massironi, G. Naletto, N. Oklay, M. Pajola, A. Pommerol, F. Preusker, F. Scholten, X. Shi, N. Thomas, I. Toth, C. Tubiana and J.-B. Vincent

Science **354** (6319), 1566-1570.
DOI: 10.1126/science.aag2671originally published online November 17, 2016

Rosetta observes sublimating surface ices

Comets are "dirty snowballs" made of ice and dust, but they are dark because the ice sublimates away, leaving some of the dust behind on the surface. The Rosetta spacecraft has provided a close-up view of the comet 67P/Churyumov-Gerasimenko as it passes through its closest point to the Sun (see the Perspective by Dello Russo). Filacchione *et al.* detected the spectral signature of solid CO_2 (dry ice) in small patches on the surface of the nucleus as they emerged from local winter. By modeling how the CO_2 sublimates, they constrain the composition of comets and how ices generate the gaseous coma and tail. Fornasier *et al.* studied images of the comet and discovered bright patches on the surface where ice was exposed, which disappeared as the ice sublimated. They also saw frost emerging from receding shadows. The surface of the comet was noticeably less red just after local dawn, indicating that icy material is removed by sunlight during the local day.

Science, this issue p. 1563, p. 1566; see also p. 1536

Science (print ISSN 0036-8075; online ISSN 1095-9203) is published by the American Association for the Advancement of Science, 1200 New York Avenue NW, Washington, DC 20005. The title *Science* is a registered trademark of AAAS.